Article

CO2 Reduction Promoted by Imidazole Supported on a Phosphonium-Type Ionic Liquid-Modified Au Electrode at a Low Overpotential

Go Iijima, Tatsuya Kitagawa, Akira Katayama, Tomohiko Inomata, Hitoshi Yamaguchi, Kazunori Suzuki, Kazuki Hirata, Yoshimasa Hijikata, Miho Ito, and Hideki Masuda

ACS Catal., **Just Accepted Manuscript** • DOI: 10.1021/acscatal.7b03274 • Publication Date (Web): 24 Jan 2018

CO_2 Reduction Promoted by Imidazole Supported on a Phosphonium-Type Ionic Liquid-Modified Au Electrode at a Low Overpotential

Go Iijima,[†] Tatsuya Kitagawa,[¶] Akira Katayama,[¶] Tomohiko Inomata,[¶] Hitoshi Yamaguchi,[†] Kazunori Suzuki,[†] Kazuki Hirata,[†] Yoshimasa Hijikata,[†] Miho Ito,[†] and Hideki Masuda[¶*]

[†] Advanced Research and Innovation Center, DENSO CORPORATION, 500-1 Minamiyama, Komenoki-cho, Nisshin 470-0111, Japan

[¶] Graduate School of Engineering, Nagoya Institute of Technology, Gokiso-cho, Showa, Nagoya 466-8555, Japan

*Corresponding email for H.M.: masuda.hideki@nitech.ac.jp

KEYWORDS: CO_2 reduction; methanol generation; ionic liquid-modified electrode; imidazole, SEIRAS

Abstract

The catalytic conversion of CO_2 to useful compounds is of great importance from the viewpoint of global warming and development of alternatives to fossil fuels. Electrochemical reduction of CO_2 using aromatic *N*-heterocylic molecules is a promising research area. We describe a high performance electrochemical system for reducing CO_2 to formate, methanol and CO using imidazole incorporated into a phosphonium-type ionic liquid-modified Au electrode, **imidazole@IL/Au**, at a low onset-potential of –0.32 V vs. Ag/AgCl. This represents a significant improvement relative to the onset-potential obtained using a conventional Au electrode (–0.56 V). In the reduction carried out at –0.4 V, formate is mainly generated, and methanol and CO are also generated with high efficiency at –0.6 ~ –0.8 V. The generation of methanol is confirmed by experiments using $^{13}CO_2$ to generate $^{13}CH_3OH$. To understand the reaction behavior of CO_2 reduction, we characterized the reactions by conducting potential- and time-dependent *in-situ* attenuated total reflection surface-enhanced infrared absorption spectroscopy (SEIRAS) measurements in D_2O. During electrochemical CO_2 reduction at –0.8 V, the C–O stretching band for CDOD (or COD) increases and the C=O stretching band for COOD increases at –0.4 V. These findings indicate that CO_2 reduction intermediates, CDOD (or COD) and COOD, are formed, depending on the reduction potential, to convert CO_2 to methanol and formate, respectively.

Introduction

Conversion of CO_2 to useful compounds and development of sustainable energy sources are subjects of intense global research because CO_2 is a major cause of global warming.[1-3] Alternative sources of energy will be required as fossil fuel sources that are exhausted in the future. It is envisioned that CO_2 may be useful for storing as alternative energy, such as solar, wind and other natural powers, by converting it to other fuels. A number of methods for reducing CO_2 electrochemically,[4-8] photo-catalytically[9-14] and thermally[15,16] have been proposed. Among such methods, efforts to promote electrochemical conversion of CO_2 into fuels such as CO, hydrocarbons and alcohol have attracted much attention and experienced the most progress. Since Hori *et al*. reported the electrochemical conversion of CO_2,[4] many additional researchers have engaged in electrochemical studies to further develop this field.[5-14] However, almost all reduction systems investigated thus far have a high overpotential and a low current efficiency and many of these systems produce 2-electron reduced species such as formate and CO.

Recently, Bocarsly *et al*. have proposed a unique synthetic scheme for generating methanol from CO_2 using aromatic *N*-heterocycles (ANHs) such as pyridinium.[17] In this case, the Faradic efficiency varies within the range of 5 - 90% in a manner which depends on the type of ANH. Electrode materials containing GaP as a semiconductor are poor in terms of reproducibility. Dyer *et al*. also studied CO_2 reduction using mercaptopteridine on a glassy carbon electrode to give formate, formaldehyde, and methanol.[18] Although the catalysts employed in these studies can reduce CO_2, there are many problems such as the uncertainty of the mechanism,[19-28] the catalytic efficiencies[29-31] and the conditions required for CO_2 reduction.[31] Most notably, the reaction efficiency and catalytic mechanism have not been clarified in all cases. The current efficiency is believed to be affected by the ability of the ANH to reach the electrode surface under homogeneous conditions.[23,24,32-34] Therefore, a method to improve access of ANH to the electrode to induce CO_2 reduction is required. Jai-Xing Lu *et al*. have reported electrochemical CO_2 reduction using a Pd nanoparticle composite substituted with pyridine derivatives modified on the electrode.[35,36] This system reduces CO_2 with high reactivity. However, some problems remain, including decomposition by the cleavage of ether bonds in the pyridine derivatives under the electrochemical and aqueous conditions and an inability to control entrapment of the pyridine derivatives. To develop an electrode surface appropriate for close access by ANH, an appropriate electrode space is needed. Another problem is the uncertainty with respect to reactivity of ANH with CO_2 on the electrode surface. Bocarsly *et al*. proposed a proton shuttle mechanism using pyridinium-derived protons as the proton source.[17] This scheme was later investigated experimentally and theoretically by Bocarsly *et al*. and Batista *et al*.[21,29] Carter *et al*. proposed a unique process which includes two electron/hydrogen reductions of the γ-position carbon of pyridine on the basis of theoretical calculations based on the relationship between the overpotential in CO_2 reduction and the reduction potential of ANH.[19] Although several possible mechanisms were reported, evidence to confirm the mechanism is lacking due to difficulties encountered in detecting intermediates using conventional analytical

methods.

Recently, we developed a unique Au electrode modified with a phosphonium-type ionic liquid (IL) as a self-assembled monolayer (IL/Au), which can entrap metal complexes within the vacant space generated among the IL molecules, regardless of the net charge of the complexes and without forming any chemical bonds.[37] Using the IL/Au electrode, we previously succeeded in promoting four-electron reduction of dioxygen by the diiron(II) complex entrapped in the vacant space between the IL molecules.[38] This arrangement could also be applied to retain a portion of the catalysts in close proximity to the electrode surface at the nano level and to effectively promote electron transfer to the catalyst in the self-assembled monolayer. Ionic liquids are known to adsorb CO_2 with high efficiency and stabilize the activated CO_2 reduction intermediates.[39,40] Use of the electrode system is expected to address problems in CO_2 reduction. In this study, we employed the IL/Au electrode incorporated with ANH (**ANH@IL/Au**) (Scheme 1), and using **ANH@IL/Au**, we performed the electrochemical reduction of CO_2. It is desirable to retain ANH on the substrate without any direct binding to promote effective electron transfer from Au to ANH and/or CO_2. We evaluated the electrochemical reduction of CO_2 and the reaction products using this **ANH@IL/Au** electrode. Fortunately, we succeeded in reduction of CO_2 to formate, methanol and CO in a high yield at a low overpotential. We also studied the CO_2-reduction behavior on the **ANH@IL/Au** by using potential-dependent and time-dependent *in-situ* attenuated total reflection surface-enhanced infrared absorption spectroscopy (ATR-SEIRAS). We propose a molecular mechanism which appears to be responsible for inducing reduction of CO_2 at a relatively low overpotential in our system.

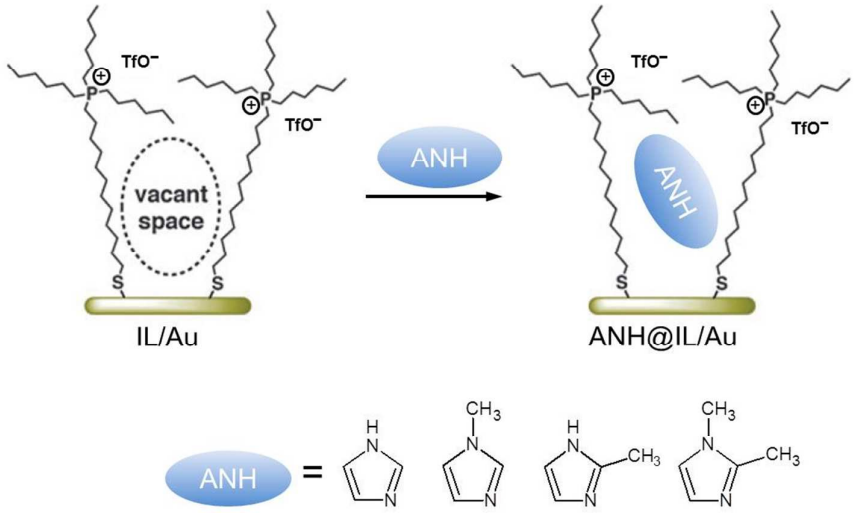

Scheme 1. Schematic illustration of the procedure for incorporation of ANH into the IL/Au electrode

Results and Discussion

Electrochemical CO_2 reduction on bare Au and ANH@IL/Au electrodes

It was deemed appropriate to confirm that **ANH@IL/Au** electrodes are more effective than a bare Au

electrode in reduction of CO_2 in terms of current efficiency and generation of products. Electrochemical reduction of CO_2 was studied using a series of ANH compounds through the following two typical electrodes at pH 6.9; (a) electrochemical reduction of a homogenous solution containing 0.01 M ANH in 0.1 M $NaClO_4$ aqueous solution using a bare Au electrode and (b) electrochemical reduction using the **ANH@IL/Au** electrode in 0.1 M $NaClO_4$ aqueous solution. The ANH compounds investigated in this study are imidazole, 1-methylimidazole, 2-methylimidazole, 1,2-dimethylimidazole, pyridine, triazole, and pyrazole. In all electrochemical reduction reactions, the main product was formate, which was detected by ion chromatography, as shown in Figure 1. The current efficiency of formate generation using a bare Au electrode was less than 5% in all other ANHs. On the other hand, in **ANH@IL/Au** systems, **imidazole@IL/Au** showed the best performance for formate generation at all potentials studied (10 - 55%) relative to other **ANH@IL/Au** electrodes. Fortunately, for **imidazole@IL/Au**, both formate and methanol were detected and measured by gas chromatography as described below. Therefore, we decided to study the electrochemical CO_2 reduction using imidazole in detail.

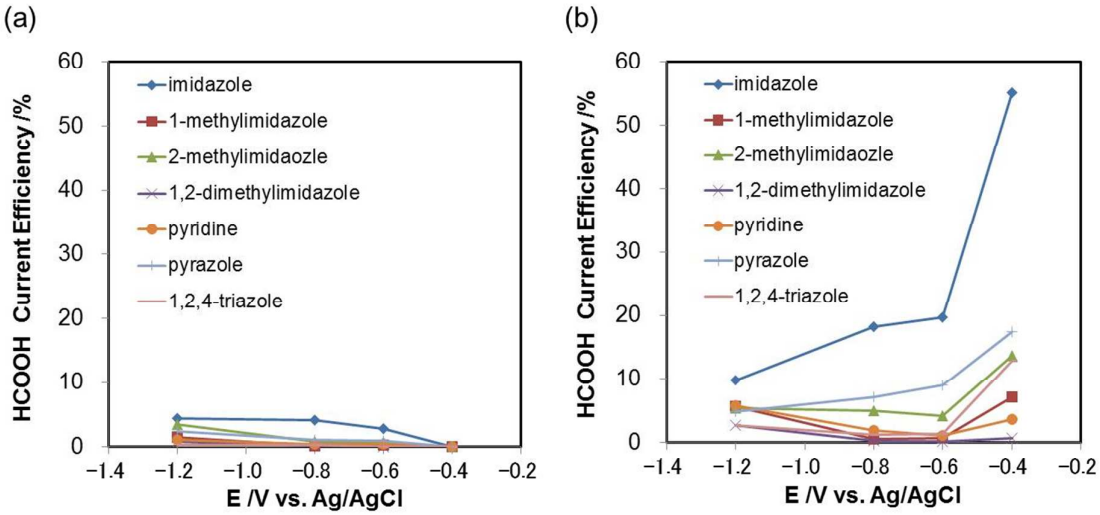

Figure 1. Current efficiencies for formate produced by CO_2 reduction in the presence of several ANH compounds. (a) Bare Au electrode and (b) **ANH@IL/Au** electrode

Overpotential for CO_2 reduction using bare Au and IL/Au with and without imidazole

We studied the electrochemical behavior of CO_2 reduction using a bare Au electrode and an IL/Au electrode with and without imidazole in a 0.1 M $NaClO_4$ aqueous solution by cyclic voltammetry (CV) in the range of 0.3 ~ –0.8 V vs. Ag/AgCl under CO_2 (Figure 2) to confirm that imidazole plays a role in reducing the overpotential for CO_2 reduction. In the reaction systems without imidazole, both the bare Au electrode and the IL/Au electrode systems have an onset-potential at –0.60 V, indicating that some extent of CO_2 reduction occurs on the Au electrode surface at this potential. The onset-potential of CO_2 reduction by the bare Au electrode in the presence of imidazole was observed at –0.56 V vs. Ag/AgCl, which is comparable to

that of direct electrochemical CO_2 reduction using a Pt electrode in the presence of imidazole (–0.51 V vs. Ag/AgCl).[17,29] Surprisingly, CV measurements using the IL/Au electrode with imidazole, **imidazole@IL/Au**, under saturated CO_2 indicate a catalytic current at –0.32 V vs. Ag/AgCl, as shown in Figure 2. The onset-potential was not changed depending on the sweep rates (Figure S5). This onset-potential is significantly lower than other onset-potentials reported previously.[29,32] The significant lowering of the onset-potential means significant lowering in the overpotential of CO_2 reduction. These facts clearly indicate that both imidazole and the modified-ionic liquid contribute to lowering of the overpotential of CO_2 reduction. This clearly represents that such a low overpotential for CO_2 reduction has been observed.

In order to clarify the catalytic characteristics of imidazole for electrochemical CO_2 reduction, we compared the electrochemical CO_2 reduction among imidazole and its derivatives (1-methylimidazole, 2-methylimidazole and 1,2-dimethylimidazole). As described above (Figure 2), the onset-potential of CO_2 reduction using the **imidazole@IL/Au** electrode has a significantly lower value, which is quite surprising in comparison with other cases that indicate onset-potentials near –0.6 V vs. Ag/AgCl (Figure S6). The cathodic current, when the bare Au electrode was used, showed a relatively large value for imidazole and all its derivatives only under a CO_2 atmosphere, as shown in Figure S6. This result indicates that imidazole and its derivatives can promote CO_2 reduction in a homogeneous solution. In the case of **1-methylimidazole@IL/Au** and **1,2-dimethylimidazole@IL/Au**, any significant differences were not observed between the CV measurement results under Ar and under CO_2. On the other hand, the significant cathodic current increasing were observed for the **imidazole@IL/Au** and the **2-methylimidazole@IL/Au** systems, indicating that N-H protons were important for CO_2 reduction in IL/Au. This corresponds with the suggestion suggested previously by Yan *et al.* that both the lone pair and the N-H proton of imidazole contribute to selective CO_2 reduction.[41] In the comparison between the **imidazole@IL/Au** and the **2-methylimidazole@IL/Au** systems, the bulky methyl group in 2-methylimidazole may be the reason why the **2-methylimidazole@IL/Au** electrode system did not give a low onset-potential. This consideration is also supported by the finding that the **imidazole@IL/Au** and **2-methylimidazole@IL/Au** systems produce formate, methanol and CO with high current efficiency relative to other imidazole derivatives (Figure S7). The results obtained for systems containing pyrazole and triazole also produce formate in good yield (Figure 1). Among all CV measurements, the most significant lowering in the overpotential of CO_2 reduction was measured for the **imidazole@IL/Au** electrode. This clearly demonstrates that imidazole has some interactions, such as hydrogen bonding and van der Waals interactions, with CO_2 on the electrode.

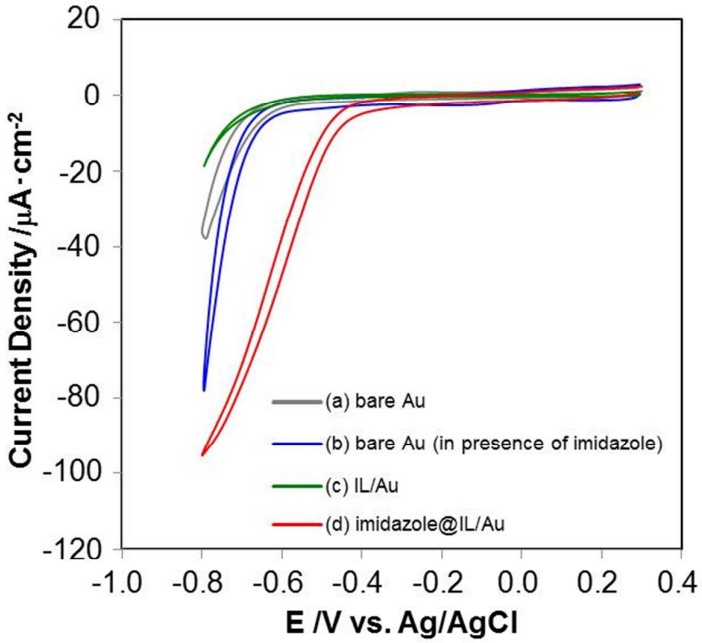

Figure 2. CV measurements under CO_2 conditions; (a) bare Au, (b) bare Au in the presence of imidazole, (c) IL/Au, (d) **imidazole@IL/Au**, as measured with a sweep rate of 10 mV/sec.

Controlled potential electrolysis measurements for CO_2 reduction

To confirm the CO_2 reduction, we conducted long running reactions using the **imidazole@IL/Au** electrode. The controlled potential electrolysis measurements conducted using **imidazole@IL/Au** as a working electrode were carried out at –0.4, –0.5, –0.6, –0.7, and –0.8 V vs. Ag/AgCl. The reaction products were analyzed by gas chromatography, ion chromatography and gas chromatography-mass spectrometry (GC-MS) to identify the reaction products of CO_2 reduction. As shown in the analytical results obtained (Figures 3, S8 and S9), formation of methanol was clearly detected. Other product not to be described in these figures was H_2, which was main product under each condition. The current efficiency of all reaction products was found to change in a manner which depends on the reaction potentials, as shown in Figure S8, and the current efficiency for methanol was 26% at –0.7 V vs. Ag/AgCl. Although the reaction using the bare Au electrode also afforded methanol, the current efficiency of CO_2 reduction was less than 1%. The comparison with the homogeneous reaction system demonstrates that this significant enhancement in catalytic behavior has been achieved by utilizing the ionic liquid self-assembled monolayer supported with imidazole. It appears that electron transfer from the electrode to imidazole and/or CO_2 has been induced by their close contact on the electrode surface. To elucidate the source of methanol obtained, we carried out the electrochemical reduction of CO_2 using the **imidazole@IL/Au** electrode system in the presence of $^{13}CO_2$, as described in the previous reports.[42,43] As expected, $^{13}CH_3OH$ was detected by GC-MS, as shown in Figure S9.

The durability of **imidazole@IL/Au** electrode was also evaluated by the plots of current density vs. time and CV and XPS measurements before and after the electrolysis (Figure S10). Fortunately, the positive shift in onset-potential and N1s peak originated from imidazole were detected even after electrolysis. These findings clearly indicate the existence of imidazoles in the **imidazole@IL/Au** electrode system after the reaction.

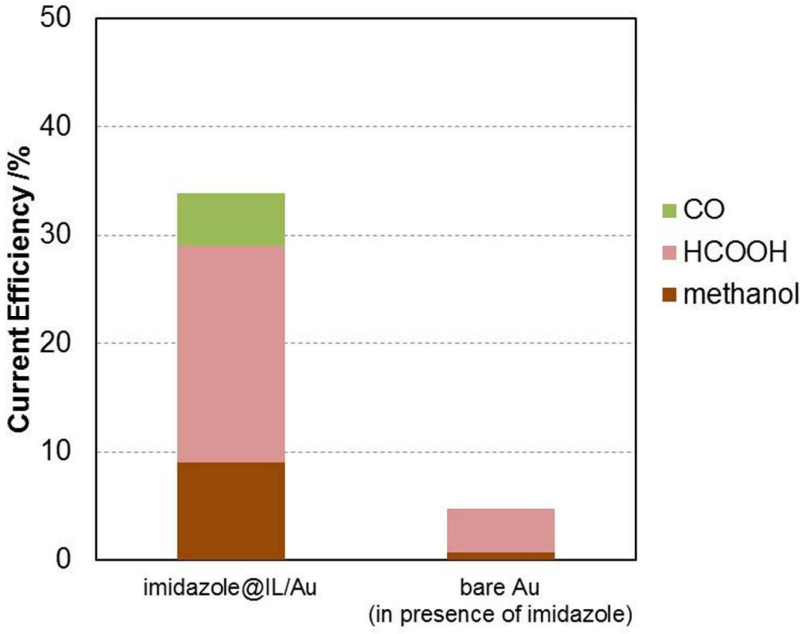

Figure 3. Current efficiencies for formate and methanol generated in the reaction at –0.8 V vs. Ag/AgCl using the **imidazole@IL/Au** electrode and the bare Au electrode in the presence of imidazole (homogeneous system).

Spectroscopic observation of CO_2 reduction on the imidazole@IL/Au surface

In order to investigate the electrochemical behavior of CO_2 reduction on the **ANH@IL/Au** electrode, we measured the *in-situ* FT-IR spectrum of the **ANH@IL/Au** electrode system using potential-dependent and time-dependent *in-situ* attenuated total reflection surface enhanced infrared absorption spectroscopy (ATR-SEIRAS).[44] This technique characterizes the surface plasmon resonance behavior of the working electrode. SEIRAS is a powerful method for observing the behavior of the molecules adsorbed on the electrode surface. In SEIRAS measurements, the intensity in an IR band of a functional group for the adsorbed molecule is enhanced 10-1000-fold by the electric field at the electrode surface.[44] Therefore, characteristic vibration modes of the molecule adsorbed on the electrode surface can be observed. The electrochemical behavior of the **imidazole@IL/Au** electrode is spectroscopically detectable using potential-dependent and time-dependent *in-situ* ATR-SEIRAS. As described above, the electrochemical measurements using **ANH@IL/Au** electrodes fabricated with several ANH compounds have demonstrated that the most efficient CO_2 reduction reaction is induced by the **imidazole@IL/Au** electrode. Potential-dependent *in-situ* ATR-SEIRAS measurements were performed in the range of 0.3 ~ −0.8 V vs.

Ag/AgCl against the working electrode in the 0.1 M $NaClO_4/D_2O$ solution on the basis of a spectrum measured at 0.3 V as background, and time-dependent *in-situ* ATR-SEIRAS at −0.4, −0.6, or −0.8 V vs. Ag/AgCl during 600 seconds on the basis of the spectrum measured at 0 seconds as the background. D_2O was employed as the solvent to prevent significant peaks of CO_2-reduction intermediates from overlapping with OH-deformation vibration peaks of H_2O. The reaction behavior of imidazole, CO_2 and ionic liquid on the electrode surfaces was monitored as described below.

(i) Reaction behavior of imidazole and CO_2 on the bare Au electrode and on the IL/Au electrode as evaluated by potential-dependent in situ ATR-SEIRAS

Figure 4(a) shows potential dependent *in situ* ATR-SEIRAS data obtained from the homogeneous system using the bare Au electrode in the presence of 0.01 M imidazole in 0.1 M $NaClO_4/D_2O$ solution under Ar and CO_2, and Figure 4(b) shows data obtained from the **imidazole@IL/Au** electrode in 0.1 M $NaClO_4/D_2O$ solution under Ar and CO_2. In the homogeneous system, the IR band assignable to the N-D stretching vibration, which was generated from H-D exchange in D_2O solution, gives rise to a peak at 2920 cm^{-1},[45] which was detected when it was swept in the negative potential region. This is more credible by detecting the peak even when we measured in the same conditions using imidazole-d_4 in D_2O solution (Figure S11(a)). This peak has increased intensity under CO_2. In contrast, the IR band assignable to D_2O observed in the range of 2400 - 2800 cm^{-1} is less intense under CO_2 relative to its intensity under Ar. This may suggest that the N-D(H) moiety of imidazole plays an important role in CO_2 reduction. In the **imidazole@IL/Au** system, some peaks observed in the range of 1900 – 2200 cm^{-1} are enhanced at negative potentials, while the N-D stretching peak at 2920 cm^{-1} is less intense than it is in the homogeneous system. Another peak, which was detected at 2100 cm^{-1} under both Ar and CO_2, is thought to be attributed to the N-D stretching mode of imidazole forming hydrogen bonds (ND-N), in place of the peak at 2920 cm^{-1} that was observed in the homogeneous system.

The difference between **imidazole@IL/Au** and homogeneous systems is that for the former, the cationic head groups of the modified-phosphonium type IL will be attracted and tilted towards the negatively-charged electrode surface at negative potentials. As mentioned above, in SEIRAS, IR peak is enhanced by resonance between vibration of compounds and Au nano-particles, in particular, vertical vibration against Au surface is more enhanced. We measured SEIRAS using IL/Au electrode (Figures S11(b), (c)), and a peak was detected at 2871 cm^{-1}, which was close to CH stretching vibration value of branched alkyl chain of IL (2855 cm^{-1}, experimental section).[46] From this finding, at an open-circuit potential, the branched alkyl chain of IL was thought to be distant from Au surface and had parallel vibration mode against Au. On the other hand, by driving to negative potential, the peak at 2871cm^{-1} was enhanced. It means that the IL tilted towards the electrode surface enhanced the resonance between vertical vibration of alkyl chain and Au nano-particles. As mentioned above, taking into consideration our proposal that the combination of the

lone pair and the N-H proton of imidazole might be crucial points to reduce CO_2, the peak at 2100 cm^{-1} (which is particularly enhanced under CO_2 as well as the peak at 2920 cm^{-1} in the homogeneous system), is attributable to the N-D stretching band of ND-N hydrogen bond between adjacent imidazoles prompted by tilted IL at negative potentials (Scheme 2). From the compounds used for experiment, this assignment is also probable. The following three compounds are attributable as a candidate of the peak; IL, CO_2 (CO_2 reduction intermediates) or imidazole. As described in the experimental section, Figures S1 and S3, IL does not have any peaks around 2100 cm^{-1}, so it could be ruled out of the candidates. Although CO_2 or CO_2 reduction intermediate was also considered as origin, they could be out of candidates because of detecting the peak at 2100 cm^{-1} under not only CO_2 but also Ar. As reported in other paper,[45,47] N-D stretching band of imidaozle-d_1 forming hydrogen bonds (ND-N) was detected at 2132cm^{-1}, which was very close to 2100 cm^{-1}. The hydrogen bonds formed between adjacent imidazoles could induce lowering of the energy requirement for accepting an electron and releasing a proton, thereby resulting in lowering of the onset-potential. The existence of imidazoles in the ionic liquid-modified Au is supported by data obtained by the XPS analysis (Figure S4); about 8 imidazole molecules are estimated to be contained in the vacant space formed by the assembly of IL against one phosphonium atom. These imidazole molecules form hydrogen bonds with each other in a previously suggested manner.[48,49]

Interestingly, only under CO_2, the peak at 1970 cm^{-1} is detected at negative potentials, which is assignable to the CO_{bridge} vibration mode. Because, in general, vibration mode of CO on substrate has two patterns, CO_{atop} and CO_{bridge}, where CO_{atop} means that C atom of CO is adsorbed on metal terminally and CO_{bridge} means that C atom of CO is adsorbed on metal with 2-hold bridge. They are observed in different wavenumber regions as follows; the former is observed over 2000 cm^{-1} and the latter is detected in the low wavenumber region of 1800 ~ 2000 cm^{-1}.[50-53] In this case, we detected the peak at 1970 cm^{-1}, so we assigned the peak as CO_{bridge}. This mode is considered to be a stable intermediate among the CO_2 reduction intermediates.[50-53] The schematic view of CO adsorption is shown in Scheme S1. In contrast, a previous study reported that a CO_{bridge} stretching peak is not usually detected in the range of 1800 - 2200 cm^{-1} using an Au electrode at negative potential.[53] This peak is detectable when a Cu electrode is used.[54] Therefore, **imidazole@IL/Au** could reduce CO_2 to stabilize CO as a CO_2 reduction intermediate more efficiently than a bare Au electrode.

In the reduction of CO_2 using **imidazole@IL/Au** system, imidazole may contribute to the CO_2 reduction through supplying protons from water. Because SEIRAS using IL/Au without imidazole did not show any D_2O peak at any potentials, as shown in Figure S11(b). On the other hand, SEIRAS using **imidazole@IL/Au** (Figure 4 (b)) gave large D_2O peak, which was enhanced at negative potentials. So, this observation clearly means that imidazole of **imidazole@IL/Au** attracted waters and conducted protons to Au for CO_2 reduction.

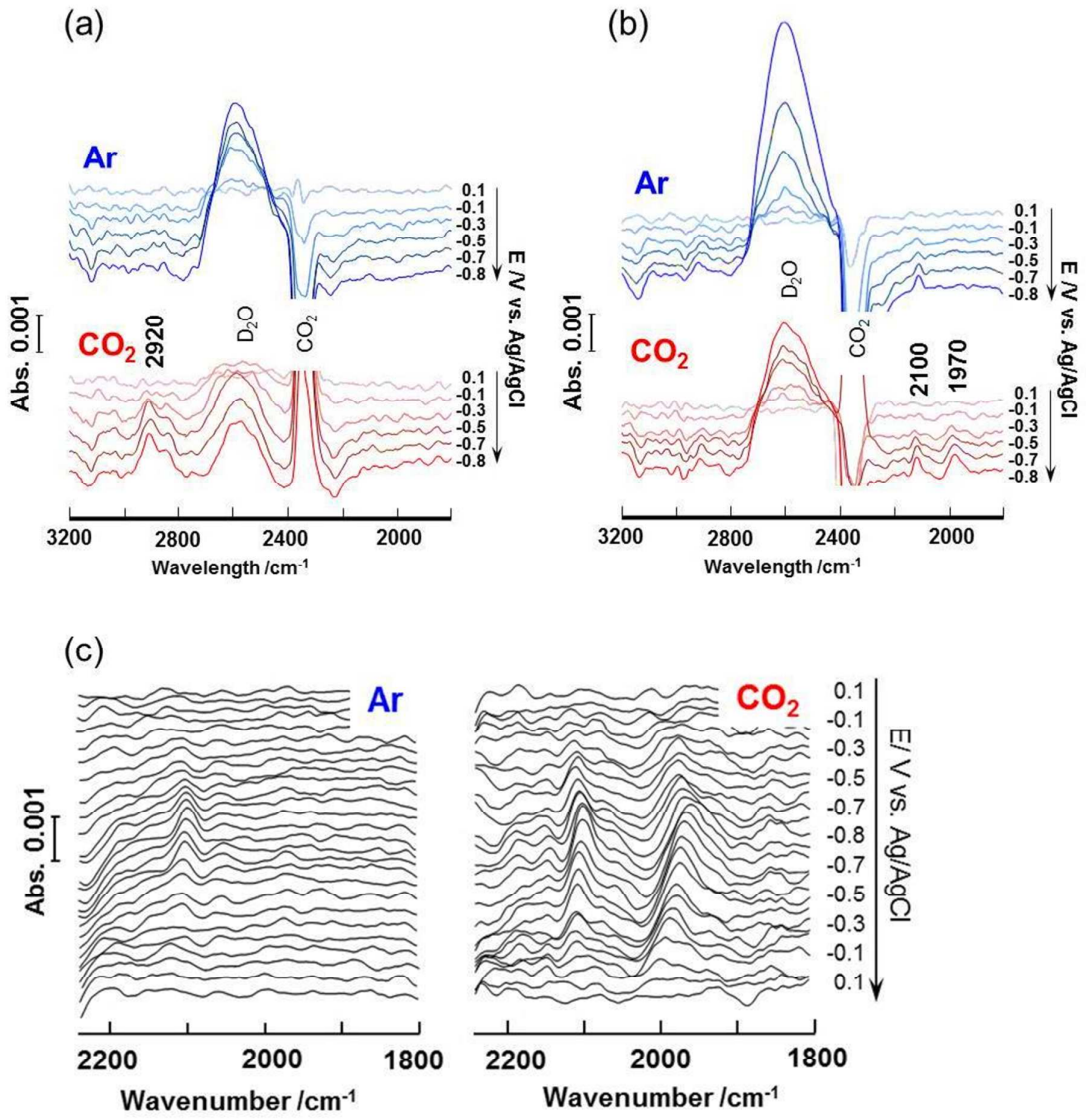

Figure 4. Potential-dependent *in situ* ATR-SEIRAS carried out in the range of 0.3 ~ –0.8 V vs. Ag/AgCl. (a) Spectra obtained using the bare Au electrode in D_2O solution containing 0.01 M imidazole (as homogeneous) under Ar or CO_2, (b) spectra obtained using the **imidazole@IL/Au** electrode under Ar or CO_2, and (c) expanded version of spectra (b) in the range of 1800 ~ 2250 cm^{-1} using the **imidazole@IL/Au** electrode under Ar or CO_2.

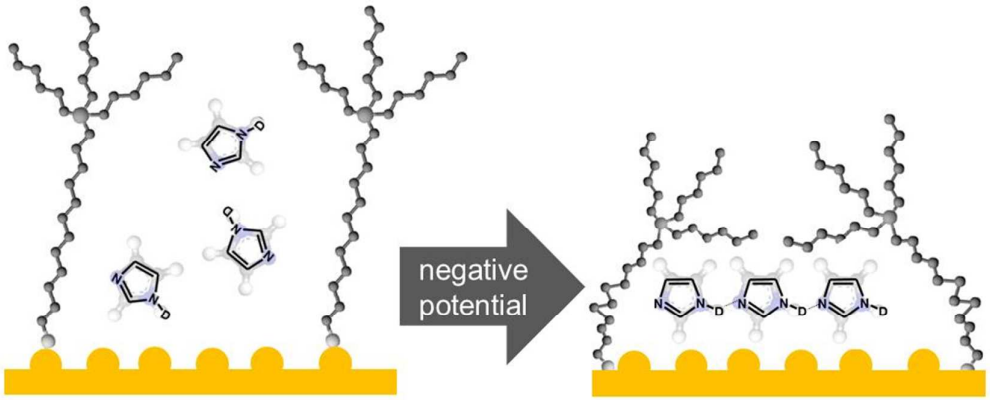

Scheme 2. Schematic illustration of forming hydrogen bonds among imidazoles accompanied by tilting of individual molecules of the phosphonium type ionic liquid at negative potential of about –0.3 V vs. Ag/AgCl.

(ii) Reaction behavior of IL/Au as evaluated by time dependent in situ ATR-SEIRAS under Ar and CO_2 conditions at –0.4, –0.6 and –0.8 V

To evaluate products treated at different potentials using **imidazole@IL/Au**, we carried out time-dependent *in situ* ATR-SEIRAS under Ar and CO_2 conditions. The results are shown in Figure 5. Under CO_2, IR peaks in the range of 1200 - 1800 cm^{-1} increase in intensity at −0.4 V and peaks in the range of 1300 ~ 1650 cm^{-1} increase at −0.6 and −0.8 V. In these cases, significant spectral changes were not observed in the upper range of 2500 cm^{-1} (Figure S12). Similarly, spectral changes were not observed for the bare Au electrode in 0.1M $NaClO_4/D_2O$ solution containing 0.01 M imidazole and for the IL/Au electrode in 0.1M $NaClO_4/D_2O$ solution (Figure S12). These results strongly suggest that the IR peaks observed using **imidazole@IL/Au** under CO_2 are attributed to intermediates or products obtained from CO_2 reduction. Also, the IR peaks attributable to the CO_{bridge} mode and the ND-N hydrogen bonds of imidazoles were not detected. This differs from the results obtained from the potential-dependent *in situ* ATR-SEIRAS measurements and indicates that the environments of the imidazole and CO_{bridge} molecules on the Au surface were not changed during the reaction time of 600 seconds. We can infer from this result that imidazole and CO are continually utilized to reduce CO_2 at each potential. Our proposal for the reaction behavior of imidazole, CO_2 and modified-ionic liquid on Au electrode at each potential is as follows.

First, the reaction at –0.4 V vs. Ag/AgCl gives rise to peaks assignable to vibration modes attributable to COOD as a CO_2 reduction intermediate; IR bands at 1740, 1371 and 1212 cm^{-1} are assignable to C=O stretching, C-O stretching and OD-deformation of COOD, respectively. [55,56] These peaks were also assigned[56] by Firet *et al.* in the electrochemical reaction of CO_2 on an Ag electrode. However, a onset-potential higher than −1.4 V vs. Ag/AgCl was required to detect them. This demonstrates that our system is able to reduce CO_2 with low activation energy.

Next, the reaction at –0.6 ~ –0.8 V vs. Ag/AgCl gives rise to IR peaks observed at 1331 and 1421 cm^{-1} as vibration modes attributed to CO_2 reduction intermediates as well. These peaks are respectively assignable to C-O stretching of DCOD or COD[57-62] and a symmetric stretching vibration mode of COO^-.[56,63-65] The former is also confirmed from the observation that methanol is generated as detected by the controlled potential electrolysis. Other peaks are assignable to products from CO_2 reduction; IR bands at 1366, 1470 and 1590 cm^{-1} are respectively assignable to C=O stretching vibrations of carbonate, adsorbed carbonate and an asymmetric stretching vibration of C=O of $DCOO^-$.[63,65,66] Generation of carbonate demonstrates effective reduction of water and production of OH^-, which continuously convert CO_2 to carbonate.[65] The peak of $DCOO^-$ appearing at 1590 cm^{-1} is usually combined with C-O stretching at 1354 cm^{-1}. Unfortunately, the IR peak at 1354 cm^{-1} overlaps with the IR band of adsorbed carbonate in our system, but it could be attributed to $DCOO^-$ from the observation that formate is detected by controlled potential electrolysis at $-0.6 \sim -0.8$ V.

As mentioned above, the results of SEIRAS also showed durability of **imidazole@IL/Au** against aqueous solution. Solubility of imidazole into aqueous solution and destruction of ND-N hydrogen bond are scientifically concerned using **imidazole@IL/Au**. However, as shown in the wide range spectra using the time dependent *in situ* SEIRAS (Figure S12(c)), there was neither change in the peaks attributable to imidazole (2300 ~ 3000 cm^{-1}) nor that to D_2O (2400 ~ 2800 cm^{-1}). Furthermore, Figures 4(a) and (b) show strong interaction between imidazole and Au substrate at negative potentials, which is opposite behavior to diffusion of imidazole into aqueous solution.

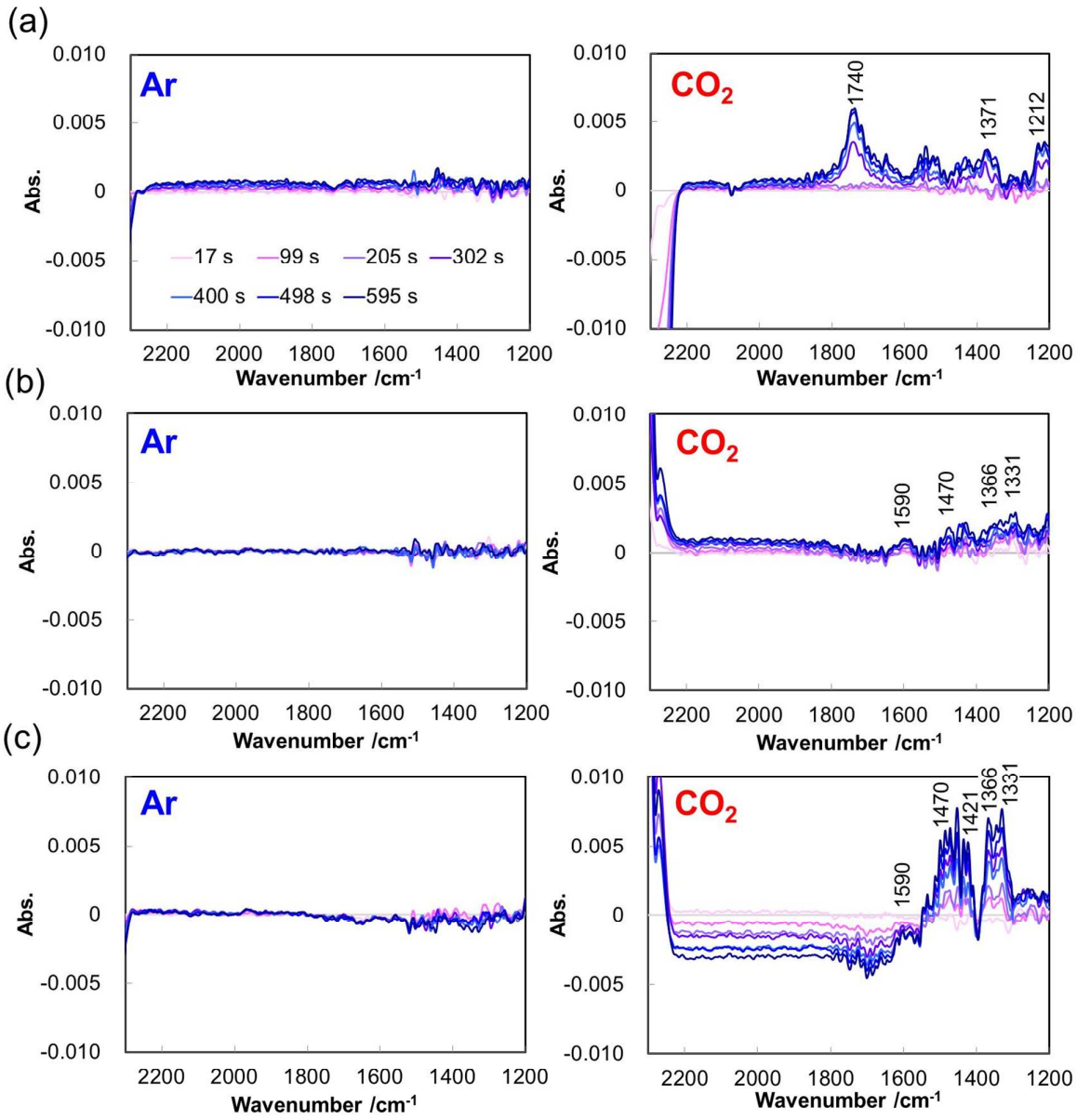

Figure 5. Time dependent *in situ* SEIRAS carried out at (a) –0.4 V, (b) –0.6 V and (c) –0.8 V vs. Ag/AgCl using the **imidazole@IL/Au** electrode under Ar or CO_2.

Mechanism of CO_2-reduction at the respective potentials

So far, two pathways for producing formate from CO_2 have been proposed in a previous report.[67] One of these pathways uses an indium substrate. It was proposed that formate is generated through oxygen-terminated formation of a metal-carbonate bond on the indium substrate. The second pathway uses a bismuth substrate. This pathway includes carbon-terminated formation of a metal-COOH bond on the bismuth substrate. In our system, COOD was detected at lower potential of −0.4 V, which leads us to

propose the following mechanism: CO_2 is reduced to formate via metal-COOH(D) with a "proton-coupled electron transfer reaction (PCET)" as proposed previously.[56,68] The PCET reaction is induced by the activated imidazole and ionic liquid. Considering that the reaction proceeds at a relatively low potential of −0.4 V, the free energy of COOH(D) bound to Au is believed to be lower in comparison with those at high potential,[61] which makes reduction unfavorable. Fang *et al.* also reported CO_2 reduction to formate using an Au electrode functionalized by 4-pyridylethylmercaptan,[69] which showed a high Faradaic efficiency to produce formate relative to bare Au. However, the onset-potential of reducing CO_2 has a higher potential at approximately −0.98 V vs. Ag/AgCl, in spite of the functionalization of Au with 4-pyridylethylmercaptan. Therefore, in our system, the detection of formate at low potential is quite a surprising result in view of the previous work.[69] When the reaction is conducted at −0.6 ~ −0.8 V, CO_2 is first reduced by one electron to form COO^-. Furthermore, with high negative potential, COO^- can be reduced to other intermediates and methanol. Interestingly, our system promotes additional reduction to methanol, although the Au substrate has been known to only reduce CO_2 to CO.[4,70-73] The reduction behavior of CO_2 bound to Au is explained by the weak binding energy of CO against Au, which has weaker binding energy than Pt and Cu.[72] In our system, the binding energy of CO against Au is assumed to be comparatively weak as well, but it is possible to reduce CO because of the efficient supply of protons provided by imidazole molecules and the effect of the ionic liquid to stabilize the CO_2 reduction intermediate.[39,73,74] The stabilization of CO_2 reduction intermediate by ionic liquid was described by Chen *et al.*, and they theoretically and experimentally demonstrated that the cationic parts of ionic liquid have a substantial stabilization effect for the activated CO_2.[73] Many CO_2 reduction intermediates possess a dipole moment or a polarizability, which would be stabilized by an electric field of the cationic parts. The detection of methanol using IL-modified Au substrate in our system is good consistent with the previously reported works.[39,73,74]

On the basis of the above results, we can propose a mechanism for reduction of CO_2 to formate and methanol. As described above, the reduction intermediates obtained at several potentials, such as CO (1970 cm^{-1} at −0.4 ~ −0.8 V), COOD (1740 cm^{-1} at −0.4 V), COO^- (1421 cm^{-1} at −0.8 V) and DCOD (or COD) (1331 cm^{-1} at –0.8 V), were observed depending on the specific operating potential. These species are converted to formate or methanol by the controlled potential electrolysis. These observations were accompanied by an increase in intensity of the IR peak at 2100 cm^{-1} which is assignable to the N-D stretching vibration of imidazole molecules forming hydrogen bonds with each other. We propose the reaction scheme illustrated in Scheme 3. In the first step, imidazole molecules are incorporated into the self-assembled ionic liquid monolayer of the **imidazole@IL/Au** electrode. In the next step, which is driven by sweeping of the electrode potential to a negative region, the cationic head groups of the phosphonium type ionic liquid are attracted towards the negatively-charged electrode. The cationic head groups retain the imidazole molecules and induce formation of hydrogen bonds between adjacent imidazole molecules. These interactions between the imidazole molecules contribute to the release of protons from the imidazole

molecules which are used to reduce CO_2 selectively. In the third step, the CO_2 reduction intermediates are stabilized by forming an ion pair with the tilted cationic ionic liquid, as was observed by *in situ* ATR-SEIRAS. Interestingly, at low potential, the tilting of ionic liquid molecules to constrain imidazole molecules and induce formation of hydrogen bonds between the induces the reduction of CO_2 in the PCET reaction.

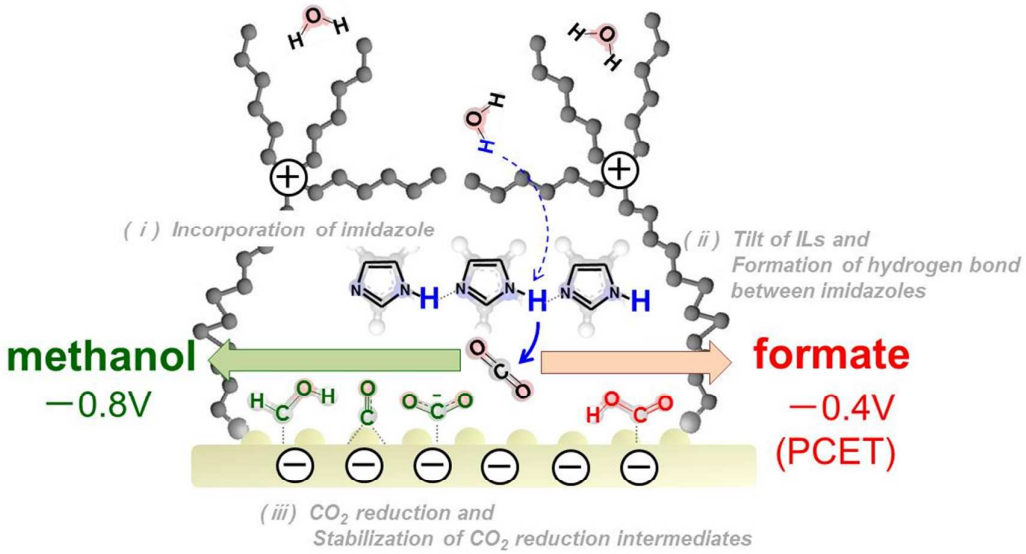

Scheme 3. Schematic illustration of the possible reactions among imidazole, CO_2 and the phosphonium type ionic liquid on the Au electrode. (i) Imidazole molecules are incorporated into the IL/Au electrode to form **imidazole@IL/Au**, (ii) when induced to negative potentials, ILs are tilted toward the electrode, which promote the formation of hydrogen bonds among imidazole molecules, and (iii) CO_2 is reduced on Au surface with supply of protons from imidazoles to begin to generate formate and methanol at -0.4 and -0.8 V, respectively.

Experimental

Synthesis of the phosphonium type ionic liquid

The phosphonium-type ionic liquid (IL) was synthesized by the previous method[37] and purified by silica gel chromatography. The preparation of IL was confirmed by NMR spectroscopy and FT-IR spectroscopy.

Preparation of the ionic liquid with the disulfide group

The procedures are as follows (see also the summary in Scheme S2).

Preparation of 12-bromododecyl(trihexyl)phosphonium bromide

1,12-dibromododecane (18.3 mmol, 6004.7 mg) was completely dissolved in toluene (60 mL) under Ar. A toluene solution (60 mL) of trihexylphosphine (18.3 mmol, 5242.5 mg) was added dropwise to this

solution over the course of 2 h. The resultant solution was stirred for 68 h under Ar at room temperature, and then the reaction mixture was evaporated. The resulting highly viscous yellow oil was purified by silica gel column chromatography (eluent: AcOEt/MeOH = 9/1). After evaporation to dryness, a viscous yellow oil was obtained. Yield 46.3%. ^{1}H-NMR (300 MHz, $CDCl_3$, *vs*. TMS): 0.90 (m, 9H, -CH_3), 1.20 - 2.30 (m, 44H, -CH_2-), 2.45 (m, 8H, -P$^+$CH_2-), 3.42 (t, 2H, BrCH_2-). FT-IR (ATR(Ge), cm^{-1}): 2954, 2926, 2855 (ν(C-H) of methylene and methyl groups), 1457 (δ(C-H) of methylene group). ESI TOF-MS (positive mode): m/z = 535.5 $[M - Br]^+$.

Preparation of 12-thiouroniumdodecyl(trihexyl)phosphonium dibromide

Thiourea (4.05 mmol, 308.3 mg) and 12-bromododecyl(trihexyl)phosphonium bromide (3.30 mmol, 2031.5 mg) were dissolved in EtOH (50 mL) and refluxed for 2 days at 90 ºC. The resultant solution was evaporated completely. The residue was dissolved in $CHCl_3$ (200 mL) and washed with H_2O (100 mL x 3) and brine (100 mL). After drying over anhydrous $MgSO_4$, a viscous pale yellow liquid was obtained by evaporation. This liquid was purified by silica gel column chromatography (eluent: $CHCl_3$/MeOH (9/1 v/v)). After evaporation to dryness, a viscous yellow liquid was obtained. Yield 33.0%. ^{1}H-NMR (300 MHz, $CDCl_3$, *vs*. TMS): 0.90 (m, 9H, -CH_3), 1.25-1.84 (m, 44H, -CH_2-), 2.31-2.58 (m, 8H, -P$^+$CH_2-), 3.39 (t, 2H, BrCH_2-), 9.00 (br, 4H, -C$^+$NH_2). FT-IR (ATR (Ge), cm^{-1}): 2956, 2923, 2853 (ν(C-H) of methylene and methyl groups), 1652 (δ(N-H) of amino group), 1458 (δ(C-H) of methylene group), 743 (ν(C-S)). ESI TOF-MS (positive mode): m/z = 529.7 $[M - H - 2Br]^+$, 265.3 $[M - 2Br]^{2+}$.

Preparation of bis[12-(trihexylphosphonium)dodecyl]disulphane dibromide

12-Thiouroniumdodecyl-(trihexyl)phosphonium dibromide (1.03 mmol, 712.5 mg) was dissolved in EtOH (30 mL). An aqueous solution (10 mL) of NaOH (2.20 mmol, 88 mg) was added to this solution. The resultant solution was stirred for 4 days at room temperature. After evaporation, the residue was dissolved in $CHCl_3$ (80 mL) and washed with H_2O (50 mL x 3) and brine (50 mL). After drying over anhydrous $MgSO_4$, the solution was evaporated completely. The resulting yellow viscous liquid was purified by silica gel chromatography (eluent: AcOEt/MeOH 9/1(v/v) (1st) and $CHCl_3$/MeOH (9/1(v/v) (2nd)). After evaporation to dryness, a yellow viscous liquid was obtained. Yield 76.5%. ^{1}H-NMR (300 MHz, $CDCl_3$, *vs*. TMS): 0.90 (m, 18H, -CH_3), 1.25-1.71 (m, 88H, -CH_2-), 2.45 (m, 16H, -P$^+$CH_2-), 2.68 (t, 4H, -SCH_2-). FT-IR (ATR (Ge), cm^{-1}): 2955, 2926, 2856 (ν(C-H) of methylene and methyl groups), 1465 (δ(C-H) of methylene group), 748 (ν(C-S)). ESI TOF-MS (positive mode): m/z = 1054.0 $[M - Br]^+$, 486.5 $[M - 2Br]^{2+}$.

Preparation of bis[12-(trihexylphosphonium)dodecyl]disulfane bis(trifluoromethanesulfonate) (1)

Bis[12-(trihexylphosphonium)dodecyl]disulphane dibromide (0.394 mmol, 446.6 mg) was dissolved in

$CHCl_3$ (25 mL). To the solution, was added EtOH solution (15 mL) of NaTfO (0.860 mmol, 148.0 mg). The resultant mixture was stirred at room temperature until the TLC spot of the starting material disappeared (eluent: $CHCl_3$/MeOH = 4/1, Rf = 0.7). After removal of the white precipitate (NaBr), the solution was evaporated completely. The residue was dissolved in $CHCl_3$ (100 mL) and washed with H_2O (100 mL x 3). After drying over anhydrous $MgSO_4$, the solution was evaporated completely. A pale yellow viscous liquid was obtained. Yield 82 %. ^{1}H-NMR (300 MHz, $CDCl_3$, *vs*. TMS): 0.90 (m, 18H, -C*H*$_3$), 1.25-1.69 (m, 88H, -C*H*$_2$-), 2.20 (m, 16H, -P$^+$C*H*$_2$-), 2.69 (t, 4H, -SC*H*$_2$-). FT-IR (ATR (Ge), cm^{-1}): 2957, 2927, 2855 (ν(C-H) of methylene and methyl groups), 1465 (δ(C-H) of methylene group), 1260 (ν(C-F) of TfO^-), 1153 sulfonate ($\nu(SO_3^-)$ of TfO^-), 1030 (ν(S=O) of TfO^-), 748 (ν(C-S)). ESI TOF-MS (positive mode): m/z = 1121.7 $[M - TfO^-]^+$, 486.3 $[M - 2\ TfO^-]^{2+}$ (Figure S1).

Preparation of the IL-modified Au (IL/Au) electrode and incorporation of imidazole into the IL/Au electrode

Preparation of IL/Au

Au film with a thickness of 2,000 Å was deposited onto a mica substrate with 14 × 14 mm at 1.0 Å s^{-1} with a JIS-300AK vacuum coater (Sinku of Technology Co., Ltd.). The Au film was annealed with a hydrogen gas flame before it was dipped into each sample solution. The IL/Au electrode was prepared according to the previously established procedure. The Au electrode modified by IL (IL/Au), was prepared by direct casting of IL onto the Au electrode with addition of a few drops over the course of a few days. After washing with EtOH and $CHCl_3$, IL/Au was obtained. The quantity of IL molecules modified on Au(111) was evaluated by electrochemical desorption,[75] which was scanned from 0.2 V to −1.4 V vs. Ag/AgCl in the 0.5M KOH solution. A reduction potential peak was observed at −1.0 V (Figure S2), and the electric charge consumed by the reductive desorption of IL was calculated to be 34.6 - 62.2 μC·cm^{-2}. The calculated amount of IL modified on Au(111) is 8.3 x 10^{-10} mol/cm^2.

Preparation of ANH@IL/Au

The **ANH@IL/Au** electrode, which was treated with both ionic liquid and ANH for immobilization of the compounds onto the Au substrate, was obtained by immersing IL/Au into Milli Q water containing 0.01 M ANH for 7 days. The incorporation of ANH (imidazole derivatives, pyridine, pyrazole, and triazole) into IL/Au was carried out by immersing the IL/Au substrate in an aqueous solution (pH 6.9) containing 0.01 M imidazole or other ANH compounds for a few days. Characterization of **imidazole@IL/Au** was performed by RAS-IR measurements (Figure S3), and the presence of imidazole held in the IL/Au cavity was confirmed by detecting an N-C stretching vibration peak at 1450 cm^{-1}. Then, the amount of imidazole incorporated into IL/Au was also determined by low temperature XPS measurements (Figure S4). At room temperature, imidazole was evaporated under high vacuum in an XPS analysis chamber. There was no

signal indicating the imidazole nitrogen atom. Therefore, we repeated the analysis at low temperature (−120 ℃), and detected signals from the imidazole nitrogen atom at 400 eV. From this measurement, it was determined that there are 1~8 molecules per IL molecule, which is estimated to be $8.3 \times 10^{-10} \sim 6.6 \times 10^{-9}$ mol/cm^2 on the surface, as estimated by comparing the peak area of the nitrogen atom with that of the phosphorus atom of IL.

Apparatus

^{1}H NMR spectra were measured on a Varian Gemini 300 MHz NMR spectrometer in $CDCl_3$ or D_2O with TMS or DSS, respectively, as internal reference standards. The concentration of each sample was adjusted to 10 mM in a sample tube (5 mmφ). Fourier transform infrared (FT-IR) spectra were recorded using a JASCO FT/IR-4200 spectrometer. Attenuated total reflection spectra were measured using a JASCO ATR PRO410-S spectrometer. Reflection-adsorption spectra were measured using a JASCO RAS-PRO410-H spectrometer. Gas-chromatography mass-spectra (GC-MS) were obtained with a JEOL JMS-Q1050GC instrument with an Inert Cap FFAP column. Gas chromatography with a flame ionization detector was performed using a Shimadzu GC-2014 instrument with an Agilent Inc. B-WAXETR column. Gas chromatography with a thermal conductivity detector was performed using an Agilent Technologies 7890A instrument with an Agilent Inc. TC-Molsieve 5A column. Ionic chromatography was performed using a Thermo Scientific DIONEX IC20 Ion system with a Thermo Scientific Ion Pac AG22 column. X-Ray photoelectron spectra (XPS spectra), were measured using an ULVAC-PHI XPS PHI5000 system with Al Kα radiation (1486.6 eV). Samples were held in the analyzing holder and inserted into the front chamber. Evacuation of the chamber was started after the holder's temperature became less than –50°C. The analysis was performed at –120°C after inserting the samples into the analyzing chamber.

Electrochemistry

Electrochemical measurements were performed using a BAS ALS model 660E analyzer. Cyclic voltammetry was performed using either an Au(111) electrode or the **ANH@IL/Au** electrode as the working electrode, a Pt wire as a counter electrode and Ag/AgCl (3 M NaCl) as reference electrode. An aqueous solution of 0.1 M $NaClO_4$ was used as the electrolyte.

Controlled potential electrolysis of CO_2 using ANH

The homogeneous reaction was performed using Milli-Q water containing 0.1 M $NaClO_4$ and 0.01 M ANH. Pt plate and Au plate were used as counter and working electrodes, respectively. The potentials of the working electrode were –0.4, –0.6, –0.8, and –1.2 V vs. Ag/AgCl, and the reaction time was 2.5 hrs. The electrochemical reduction reactions using the **ANH@IL/Au** electrode were carried out at –0.4, –0.6, –0.8, and –1.2 V vs. Ag/AgCl in Milli Q water containing 0.1 M $NaClO_4$, and the reaction time was 2.5 hrs.

The ANH molecules evaluated are imidazole, 1-methylimidazole, 2-methylimidazole, 1,2-dimethylimidazole, pyridine, triazole, and pyrazole. The analyses of formate, methanol and gas products from electrolysis were performed by Ionic chromatography, Gas chromatography (Shimadzu GC-2014) and Gas chromatography (Agilent Technologies 7890A), respectively. Amounts of these products were estimated from each calibration curve using the standard compounds for each instrument.

Preparation of the electrode for SEIRAS measurements

The electrode was prepared for SEIRAS measurements as illustrated in Scheme S3. The Si ATR prism used for SEIRAS measurements was polished using 0.05 mmφ alumina for about 10 minutes and subsequently cleaned in Milli-Q water using an ultrasonic sonicator for 30 minutes. The surface of the Si prism was etched with a 40% NH_4F solution, cleaned with Milli-Q water, and continuously treated with 5 mM $Na(AuCl_4)\cdot 2H_2O$, 50 mM Na_2SO_3, 15 mM $Na_2S_2O_3$, 15 mM NH_4Cl, and 1 wt% HF solution at 60°C to prepare the Au thin layer on the Si prism. The resistance of the plated Au was about 10 ohms. Immobilization of ionic liquids and ANH onto the Au thin layer was performed by dipping the electrode into aqueous solutions containing these compounds.

Characterization of the SEIRAS film

The characterization of the SEIRAS film was employed using cyclic voltammogram with Au film prepared on a Si ATR prism in 0.1 M H_2SO_4 aqueous solution. Scan rate was 20 mV s^{-1}. Active surface area was calculated by integrating the reduction peak of Au oxide for a theoretical value of 444 μC/cm^2 required for reducing Au oxide monolayer (Figure S13).[76] The roughness factor of Au film employed for SEIRAS measurement was estimated as 4.18.

Measurements of *in-situ* ATR-SEIRAS

Potential-dependent and time-dependent *in-situ* ATR-SEIRAS measurements were performed using the **ANH@IL/Au** electrode, which was immobilized with both IL and ANH on the Au thin layer plated on a hemispherical Si ATR prism. SEIRA spectra were recorded in the Kretschmann attenuated total reflection (ATR) configuration[41] using a JASCO FT/IR4200 Fourier transform IR spectrometer equipped with a HgCdTe (MCT) detector, in which the resolution of spectra is 4 cm^{-1}. Electrochemical measurements were carried out using a BAS ALS600 series electrochemical analyzer. Potential-dependent and time-dependent measurements were performed using either the bare Au electrode plated on a Si ATR-prism or the **ANH@IL/Au** electrode as the working electrode, using a Pt wire as a counter electrode and an Ag/AgCl (3 M NaCl) as a reference electrode. A 0.1 M $NaClO_4/D_2O$ solution was used as the electrolyte, which was saturated with either Ar or CO_2.

Conclusion

In summary, we developed a system for reducing CO_2 at a low onset-potential (–0.32 V vs. Ag/AgCl), and succeeded in generation of methanol at –0.7 V with high current efficiency (26% yield) using an imidazole-incorporated ionic liquid-modified Au electrode in an aqueous solution. This system represents a significant improvement over the previous system which employs pyridine/pyridinium ion on an Au electrode and is not capable of producing methanol for reduction of CO_2.[32] In the present system, we determined that formation of hydrogen bonds among imidazole molecules in ionic liquid on Au substrate is a key aspect of the electrochemical CO_2 reduction. In order to elucidate the CO_2 reduction behavior for the **imidazole@IL/Au** electrode, we characterized the interaction/reaction behavior of molecules on the electrode by conducting *in situ* ATR-SEIRAS measurements. Our proposed mechanism of CO_2 reduction to formate and methanol at different potentials (Scheme 3) is based on data obtained from a combination of time-dependent and potential-dependent *in situ* ATR-SEIRAS methods. We believe that the mechanism for altering electron transfer properties identified in this work will contribute to the development of high performance catalysts for conversion of CO_2 to useful compounds.

Supporting Information

The Supporting Information is available free of charge on the ACS Publications website at DOI: @@@@@@@@@@@@.

> Additional spectroscopic details and schemes (PDF)

Acknowledgments

This work was supported in part by the Japan Society for the Promotion of Science (JSPS) through the Program for Advancing Strategic International Networks to Accelerate the Circulation of Talented Researchers and the Japan Society for the Promotion of Science (JSPS) for a Grant-in-Aid for Scientific Research (B)(C) (No. 16H04117, 15K05606).

References

1. Albo J.; Alvarez-Guerra M.; Castañoa P.; Irabien A. *Green Chem*. **2015**, *17*, 2304−2324.
2. Kim J.; Johnson T. A.; Miller J. E.; Stecheld E. B.; Maravelias C. T.; *Energy Environ. Sci.* **2012**, *5*, 8417−8429.
3. Lee S.; Kim D.; Lee J. *Angew. Chem., Int. Ed.* **2015**, *54*, 14701−14705.
4. Hori Y.; Kikuchi K.; Suzuki S. *Chem. Lett.* **1985**, *14*, 1695−1698.
5. Lewis N. S.; Nocera D. G. *Proc. Natl. Acad. Sci. U. S. A.* **2006**, *103*, 15729−15735.
6. Nakata K.; Ozaki T.; Terashima C.; Fujishima A.; Einaga Y. *Angew. Chem., Int. Ed.* **2014**, *53*, 871−874.
7. Qiao J.: Liu Y.; Hong F.; Zhang J. *Chem. Soc. Rev.* **2014**, *43*, 631−675.

8. Costentin C.; Robert M.; Savéant J.-M. *Chem. Soc. Rev.* **2013**, *42*, 2423−2436.
9. Licht S. *Adv. Mater*. **2011**, *23*, 5592−5612.
10. Roy S. C.; Varghese O. K.; Paulose M.; Grimes C. A. *ACS Nano* **2010**, *4*, 1259−1278.
11. Lewis N. S. *Science* **2007**, *315*, 798−801.
12. Kumar B.; Llorente M.; Froehlich J.; Dang T.; Sathrum A.; Kubiak C. P. *Annu. Rev. Phys. Chem.* **2012**, *63*, 541−569.
13. Tran P. D.; Wong L. H.; Barber J.; Loo J. S. C. *Energy Environ. Sci.* **2012**, *5*, 5902−5918.
14. Yui T.; Tamaki Y.; Sekizawa K.; Ishitani O. *Top Curr. Chem.* **2011**, *303*, 151−184.
15. Balaraman E.; Gunanathan C.; Zhang J.; Shimon L. J. W.; Milstein D. *Nat. Chem.* **2011**, *3*, 609−614.
16. Centi G.; Perathoner S. *Catal. Today* **2009**, *148*, 191−205.
17. Cole E. B.; Lakkaraju P. S.; Rampulla D. M.; Morris A. J.; Abelev E.; Bocarsly A. B. *J. Am. Chem. Soc.* **2010**, *132*, 11539−11551.
18. Xiang D.; Magana D.; Dyer R. B. *J. Am. Chem. Soc.* **2014**, *136*, 14007−14010.
19. Keitha J. A.; Carter E. A. *Chem. Sci.* **2013**, *4*, 1490−1496.
20. Marjolin A.; Keith J. A. *ACS Catal.* **2015**, *5*, 1123−1130.
21. Ertem M. Z.; Konezny S. J.; Araujo C. M.; Batista V. S. *J. Phys. Chem. Lett.* **2013**, *4*, 745−748.
22. Lim C.-H.; Holder A. M.; Hynes J. T.; Musgrave C. B. *J. Phys. Chem. Lett.* **2015**, *6*, 5078−5092.
23. Peroff A. G.; Weitz E.; Van Duyne R. P. *Phys. Chem. Chem. Phys.* **2016**, *18*, 1578−1586.
24. Lim C.-H.; Holder A. M.; Musgrave C. B. *J. Am. Chem. Soc.* **2013**, *135*, 142−154.
25. Costentin C.; Canales J. C.; Haddou B.; Savéant J.-M *J. Am. Chem. Soc.* **2013**, *135*, 17671−17674.
26. Yan Y.; Zeitler E. L.; Gu J.; Hu Y.; Bocarsly A. B. *J. Am. Chem. Soc.* **2013**, *135*, 14020−14023.
27. Dridi H.; Comminges C.; Morais C.; Meledje J.-C.; Kokoh K. B.; Costentin C.; Savéant J.-M. *J. Am. Chem. Soc.* **2017**, *139*, 13922–13928.
28. Dunwell M.; Yan Y.; Xu B. *ACS Catal.* **2017**, *7*, 5410–5419.
29. Liao K.; Askerka M.; Zeitler E. L.; Bocarsly A. B.; Batista V. S. *Top. Catal.* **2015**, *58*, 23−29.
30. Portenkirchner E.; Enengl C.; Enengl S.; Hinterberger G.; Schlager S.; Apaydin D.; Neugebauer H.; Knör G.; Sariciftci N. S. *ChemElectroChem* **2014**, *1*, 1543−1548.
31. Rybchenko S. I.; Touhami D.; Wadhawan J. D.; Haywood S. K. *ChemSusChem.* **2016**, *9*, 1660−1669.
32. Lucio A. J.; Shaw S. K. *J. Phys. Chem. C* **2015**, *119*, 12523−12530.
33. Lebegue E.; Agullo J.; Morin M.; Belanger D. *ChemElectroChem* **2014**, *1*, 1013−1017.
34. Barton Cole E. E.; Baruch M. F.; L'Esperance R. P.; Kelly M. T.; Lakkaraju P. S.; Zeitler E. L.; Bocarsly A. B. *Top. Catal.* **2015**, *58*, 15−22.
35. Yang H.-P.; Qin S.; Wang H.; Lu J.-X. *Green Chem.* **2015**, *17*, 5144−5148.
36. Yang H.-P.; Yue Y.-Na; Qin S.; Wang H.; Lu J-X. *Green Chem.* **2016**, *18*, 3216−3220.
37. Kitagawa T.; Inomata T.; Funahashi Y.; Ozawa T.; Masuda H. *Chem. Commun.* **2013**, *49*, 10184−10186.

38. Kitagawa T.; Nishino J.; Inomata T.; Ozawa T.; Funahashi Y.; Masuda H. *Chem. Commun*. **2016**, *52*, 4780−4783.

39. Rosen B. A.; Salehi-Khojin A.; Thorson M. R.; Zhu W.; Whipple D. T.; Kenis P. J. A.; Masel R. I. *Science* **2011**, *334*, 643−644.

40. Aki S. N. V. K.; Mellein B. R.; Saurer E. M.; Brennecke J. F. *J. Phys. Chem. B* **2004**, 108, 20355−20365.

41. Yan Y.; Gu J.; Bocarsly A. B. *Aerosol Air Qual. Res.* **2014**, *14*, 515–521.

42. Seshadri G.; Lin C.; Bocarsly A. B. *J. Electro. Chem.* **1994**, *372*, 145−150.

43. Boston D. J.; Xu C.; Armstrong D. W.; MacDonnell F. M. *J. Am. Chem. Soc.* **2013**, *135*, 16252−16255.

44. Osawa M. *Bull. Chem. Soc. Jpn.* **1997**, *70*, 2861−2880.

45. Perchard C.; Bellocq A. M.; Novak A. *J. Chim. Phys.* **1965**, *62*, 1344–1358.

46. Grossutti M.; Leitch J. J.; Seenath R.; Karaskiewicz M.; Lipkowski J. *Langmuir* **2015**, *31*, 4411−4418.

47. Sister M. C.; Walter J. L. *Spectrochimica Acta* **1968**, *24*, 237−252.

48. Rodriguez J.; Elola M. D.; Laria D. *J. Phys. Chem. B* **2015**, *119*, 9123−9128.

49. Costa P. S.; Miller D. P.; Teeter J. D.; Beniwal S.; Zurek E.; Sinitskii A.; Hooper J.; Enders A. *J. Phys. Chem. C* **2016**, *120*, 5804−5809.

50. Furuya N.; Motto S.; Kunimatsu K. *J. Electroanal. Chem.* **1988**, *239*, 347−360.

51. Miki A.; Yeb S.; Osawa M. *Chem. Comm.* **2002**, *21*, *1500*−1501.

52. Wuttig A.; Yaguchi M.; Motobayashi K.; Osawa M.; Surendranath Y. *Proc. Natl. Acad. Sci. U. S. A.* **2016**, *113*, E4585–E4593.

53. Dunwell M.; Lu Q.; Heyes J. M.; Rosen J.; Chen J. G.; Yan Y.; Jiao F.; Xu B. *J. Am. Chem. Soc.* **2017**, *139*, 3774−3783.

54. Wuttig A.; Liu C.; Peng Q.; Yaguchi M.; Hendon C. H.; Motobayashi K.; Ye S.; Osawa M.; Surendranath Y. *ACS Cent. Sci.* **2016**, *2*, 522−528.

55. Xia X. H.; Liess H. D.; Iwasita T. *J. Electroanal. Chem.* **1997**, *437*, 233−240.

56. Firet N. J.; Smith W. A. *ACS Catal.* **2017**, *7*, 606–612.

57. Li M.; Liu P.; Adzic R. R. *J. Phys. Chem. Lett.* **2012**, *3*, 3480−3485.

58. Koziol L.; Mozhayskiy V. A.; Braams B. J.; Bowman J. M.; Krylov A. I. *J. Phys. Chem. A* **2009**, *113*, 7802−7809.

59. Iwasita T.; Nart F. C. *Pro. Surf. Sci.* **1997**, *55*, 271−340.

60. Bowman J. M.; Bittman J. S.; Harding L. B. *J. Chem. Phys.* **1986**, *85*, 911−921.

61. Liu X.; Xiao J.; Peng H.; Hong X.; Chan K.; Nørskov J. K. *Nature Commun.* **2017**, 15438.

62. Xiao H.; Cheng T.; Goddard III W. A.; Sundararaman R. *J. Am. Chem. Soc.* **2016**, *138*, 483−486.

63. Arihara K.; Kitamura F.; Ohsaka T.; Tokuda K. *J. Electroanal. Chem.* **2001**, *510***,** 128−135.

64. Sandoval A. P.; Orts J. M.; Rodes A.; Feliu J. M. *J. Phys. Chem. C* **2011**, *115*, 16439−16450.

65. Figueiredo M. C.; Ledezma-Yanez I.; Koper M. T. M. *ACS Catal.* **2016**, *6*, 2382−2392.

66. Rodriguez P.; Kwon Y.; Koper M. T. M. *Nature Chem.* **2014**, *4*, 177–182.

67. Pander III J. E.; Baruch M. F.; Bocarsly A. B. *ACS Catal.* **2016**, *6*, 7824−7833.

68. Kortlever R.; Shen J.; Schouten K. J. P.; Calle-Vallejo F.; Koper M. T. M. *J. Phys. Chem. Lett.* **2015**, *6*, 4073–4082.

69. Fang Y.; Flake J. C. *J. Am. Chem. Soc.* **2017**, *139*, 3399−3405.

70. Hori Y.; Murata A.; Kikuchi K.; Suzuki S. *J. Chem. Soc., Chem. Commun.* **1987**, 728−729.

71. Chen Y.; Li C. W.; Kanan M. W. *J. Am. Chem. Soc.* **2012**, *134*, 19969−19972.

72. Shi C.; Hansen H. A.; Lausche b A. C.; Nørskov J. K. *Phys. Chem. Chem. Phys.* **2014**, *16*, 4720−4727.

73. Chen L. D.; Urushihara M.; Chan K.; Nørskov J. K. *ACS Catal.* **2016**, *6*, 7133−7139.

74. Cave E. R.; Montoya J. H.; Kuhl K. P.; Abram D. N.; Hatsukade T.; Shi C.; Hahn C.; Nørskovb J. K.; Jaramillo T. F. *Phys. Chem. Chem. Phys.* **2017**, *19*, 15856−15863.

75. Yoshimoto, S.; Ono, Y.; Kuwahara, Y.; Nishiyama, K.; Taniguchi, I. *J. Phys. Chem. C* **2016**, *120*, 15803 −15813.

76. Angerstein-Kozlowska, H.; Conway, B. E.; Hamelin, A.; Stoicoviciu, L. *Electrochim. Acta* **1986**, *31*, 1051−1061.

Table of content